

# Thermal Equivalent Circuit Modelling and Experimental Validation of Pouch-type Lithium-ion Cell

Belfun ARSLAN<sup>1,2\*</sup>, Özgün YÜCEL<sup>1</sup>, Cem Hakan YILMAZ<sup>2</sup>

<sup>1</sup>Gebze Technical University, Chemical Engineering Department  
Gebze, Kocaeli, Turkey

[b.arslan2022@gtu.edu.tr](mailto:b.arslan2022@gtu.edu.tr); [yozungun@gtu.edu.tr](mailto:yozungun@gtu.edu.tr)

<sup>2</sup>Mutlu Akü

Tuzla, Istanbul, Turkey

[barslan@mutlu.com.tr](mailto:barslan@mutlu.com.tr); [cemy@mutlu.com.tr](mailto:cemy@mutlu.com.tr)

**Abstract** - There is a growing demand for advanced energy storage systems. Lithium-ion batteries have become a high-demand energy technology due to their high energy density. However, temperature plays a crucial role in the performance, safety, and lifespan of lithium-ion batteries. Numerical models can be used to analyse thermal behaviour of Li-ion cells to improve effective thermal management system. In this study equivalent circuit model (ECM) model was used in numerical analysis. The ECM is comprised of two resistance-capacitance (RC) networks, one series resistor, and one voltage source that are all function of state-of-charge (SOC) and temperature. Hybrid pulse power characterization (HPPC) test is applied to extract the ECM parameters. Numerical and experimental tests were performed at 298.15K environmental temperature and 0.25C, 0.5C and 1C constant discharge rates. The numerical model shows good agreement with experimental test data. The developed model can be employed for battery thermal management system (BTMS) design by saving calculation costs efficiently.

**Keywords:** Pouch type Li-ion cell, Thermal model, ECM model, Validation, Temperature distribution

## 1. Introduction

Energy crises and environmental pollution have become common problems faced by all countries in the world. The advancement and adoption of electric vehicles (EVs) and battery energy storage (BES) technology serve as potent measures to address these issues. Among the essential components of EVs and BES, the battery pack assumes a crucial role in energy storage. The lithium-ion battery emerges as the preferred choice for battery packs owing to its numerous advantages, including long cycle life, a high voltage range, a low self-discharge rate, lightweight design, and absence of memory effect[1].

However, lithium-ion batteries are sensitive to temperature variations during operation. As illustrated in Fig. 1., the ideal operating temperature for lithium-ion batteries falls within the range of 288.15K to 308.15K. Temperatures exceeding 308.15K intensify internal side reactions, leading to capacity deterioration and reduced battery lifespan. Additionally, incidents of fire or explosions in EVs due to overheating batteries are frequently reported, prompting significant concerns regarding EV safety. Conversely, at temperatures below 288.15K, discharge capacity diminishes significantly due to increased internal resistance and slower reaction kinetics, resulting in a notably shorter driving range. Consequently, effective thermal management becomes critical for maintaining battery performance and ensuring safety throughout the battery's lifecycle [2].

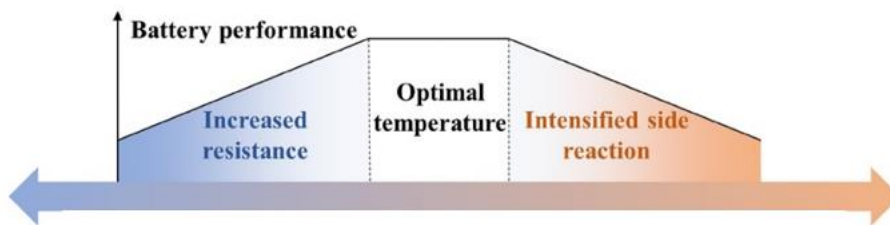


Fig. 1: Optimum operating temperature of Li-ion battery [3].

Modelling and simulation of lithium-ion batteries are becoming increasingly important in developing a fundamental understanding of electrochemical performances and thermal properties to improve battery thermal management systems. Generally, a thermal model integrates three different approaches to characterize the thermal performance of the battery: a semiempirical model, an equivalent circuit model (ECM), and an electrochemical model. The first two models focus on thermal behaviour while ignoring the complex physics of electrochemistry, such as the distribution of electronic and ionic currents and temperature gradients. However, a combined electrochemical-thermal model provides valuable insight into the performance of a battery by considering both its thermal behaviour and electrochemical phenomenon. This model proves useful for battery component design and provides detailed information on electrochemical behaviour. However, its extensive computational requirements make it unsuitable for full-cell-scale battery design for thermal management purposes [4].

In this research, the thermal behaviour of the pouch-type polymer NMC Li-ion cell was investigated as experimental and numerical studies at room temperature and different current rates. ECM model was used in numerical analysis.

## 2. Test Methodology and Description

### 2.1. Thermal Model

The energy balance equation can be written as follows.

$$\rho C_p \frac{\partial T}{\partial t} = \nabla(k\Delta T) + \dot{q} - \dot{q}_{dis} \quad (1)$$

Where  $\rho$  is the density,  $C_p$  is the heat capacity ( $\text{Jkg}^{-1}\text{K}^{-1}$ )  $T$  is the temperature (K),  $t$  is the time (sec), and  $k$  is the thermal conductivity ( $\text{W m}^{-1} \text{K}^{-1}$ ),  $\dot{q}$  ( $\text{W/m}^3$ ) is the heat source per unit volume in the battery.

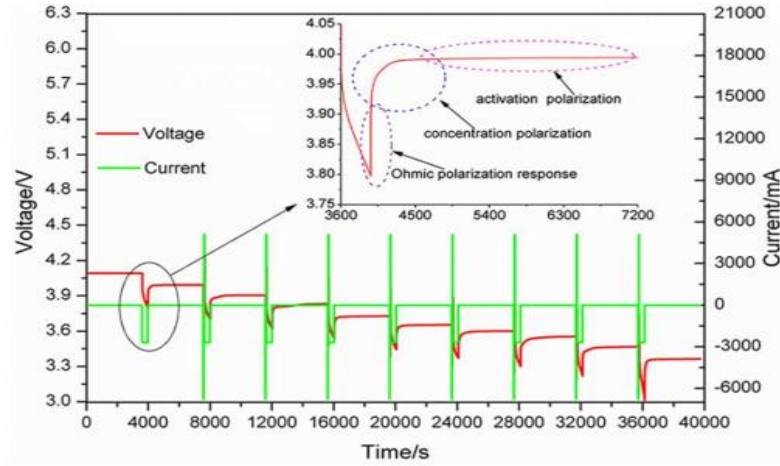
$$\dot{q} = \dot{q}_{rev} + \dot{q}_{pol} + \dot{q}_{ohm} \quad (2)$$

$\dot{q}$  is equal sum of reversible heat ( $\dot{q}_{rev}$ ), polarization heat ( $\dot{q}_{pol}$ ), and ohmic heat ( $\dot{q}_{ohm}$ ). In which,  $\dot{q}_{rev}$  is caused by the entropy change of electrode materials,  $\dot{q}_{pol}$  is related to the polarization voltage during discharge process, and  $\dot{q}_{ohm}$  is derived by the electrical ohmic heat in the solid phase as well as ionic ohmic heat in the electrolyte. In addition,  $\dot{q}_{dis}$ , which is determined by Newton's law of cooling, is the convective heat dissipation on the outer surface of the battery. However, to avoid the disturbances caused by external cooling, the battery is assumed to be exposed to a uniform heat transfer coefficient. Therefore, the flow field calculation is ignored in this research [5].

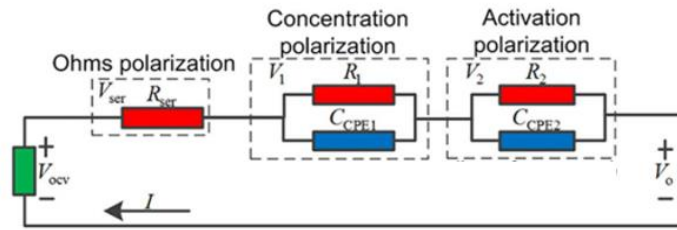
### 2.2. ECM Model

Hybrid pulse power characterization (HPPC) testing is a methodology used to determine the dynamic performance characteristics of a battery. This testing determines battery power capability over the cell's usable voltage range. It is a test profile that incorporates both discharge and regeneration pulses that take place at various states of charge (SOC), and which can be performed under various temperature stressors and current loads. In the ECM model used in numerical analysis, the necessary data about the battery was obtained by performing HPPC testing. Representing HPPC test pulses and ECM model were shown in Fig 2. HPPC testing was carried out according to the following steps after the CCCV charging step until 0% charge state.

- 1h rest
- Pulse discharge with 0.5C for 10s
- 10min rest
- Pulse charge with 0.5C for 10s
- 10min rest
- 0.2C discharge until lost 5% capacity of cell's capacity



(a)



(b)

Fig 2. (a) HPPC test of lithium-ion battery; (b) Simplified lithium-ion battery ECM based on HPPC test [6].

$R_1$ ,  $C_1$ ,  $R_2$ ,  $C_2$  are obtained from a least square fitting of the voltage curve during the relaxation period. Necessary model equations were given Eqs. (3)-(6) below [6].

$$V(t) = V_{OCV}(soc) + V_1 + V_2 - R_s(soc)I(t) \quad (3)$$

$$\frac{dV_1}{dt} = -\frac{1}{R_1(soc)C_1(soc)}V_1 - \frac{1}{C_1(soc)}I(t) \quad (4)$$

$$\frac{dV_2}{dt} = -\frac{1}{R_2(soc)C_2(soc)}V_2 - \frac{1}{C_2(soc)}I(t) \quad (5)$$

$$soc = soc_0 - \frac{\int_0^t I(t)dt}{3600Q_{Ah}} \quad (6)$$

$R_s$  (ohmic polarization) data obtained from the HPPC test as a function of state of charge is shown in Fig 3. Resistance is highest at 0.001% charge state.

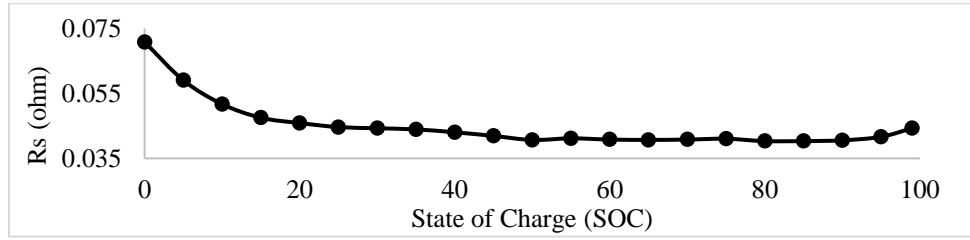


Fig 3. Rs values of NMC-polymer Li-ion cell according to SOC.

### 2.3. Experimental

Power-Xtra PX105080 NMC polymer Li-ion pouch type cell was used in the experiment. Current collectors for positive and negative electrodes are aluminium and copper respectively. Temperature tests were performed in an air-conditioning cabin at 298.15K with 0.25C, 0.5C and 1C constant discharge.



Fig 4. NMC polymer Li-ion cell.

During discharge, temperature values were measured with Pt100 temperature sensors at 5 points marked in Fig. 4. Temperature data were recorded on the JUMO LOGOSCREEN nt device. Cell properties are given in Table 1. Electrical conductivities for Uds0 and Uds1 were taken as  $3.774 \cdot 10^7$  [S/m] and  $5.998 \cdot 10^7$  [S/m] respectively [7]. Additionally, the average temperature values of the points shown in Fig. 4. were calculated in the numerical model for code verification.

Table 1: Cell Properties.

| Cell Properties                        | Value          | Unit                 |
|--|----------------|----------------------|
| Cell Capacity                          | 5.2            | Ah                   |
| Nominal Voltage                        | 3.7            | V                    |
| Charge Cut-off Voltage                 | 4.2            | V                    |
| Discharge Cut-off Voltage              | 2.75           | V                    |
| Standard Charging Current              | 0.2            | C                    |
| Standard Discharging Current           | 0.2            | C                    |
| Cell Length; Width; Thickness          | 75; 50; 10     | [mm]                 |
| Tab Length; Width; Thickness           | 11.25; 4; 0.15 | [mm]                 |
| Through Plane Thermal Conductivity [7] | 30.04          | [W/Mk]               |
| In Plane Thermal Conductivity          | 1.70           | [W/Mk]               |
| Density [7]                            | 1853.2         | [kg/m <sup>3</sup> ] |
| Heat Transfer Coefficient [7]          | 10             | [W/m <sup>2</sup> K] |
| Heat Capacity [7]                      | 987.01         | [J/kgK]              |

### 2.4. Mesh Independence and Code Validation

Mesh independence tests were performed at 0.25 C constant discharge rate, with five different element numbers, and the average maximum temperatures of cell were compared. The results of the study are showed in Fig. 5a., and the quality values of each solution are summarized in Table 2.

Table 2: Mesh qualities

| Element Number | Min Orthogonal | Max Skewness |
|----------------|----------------|--------------|
| 21761          | 0.39           | 0.26         |
| 69897          | 0.41           | 0.27         |
| 92083          | 0.44           | 0.29         |
| 183050         | 0.4            | 0.28         |
| 232445         | 0.4            | 0.28         |

In the analyses carried out in different element number, it is seen that the average maximum value of five different temperature values measured on the cell surface does not change after the 183050-element size. Fig. 5b. shows the polyhedral solution mesh structure in 183050 element size.

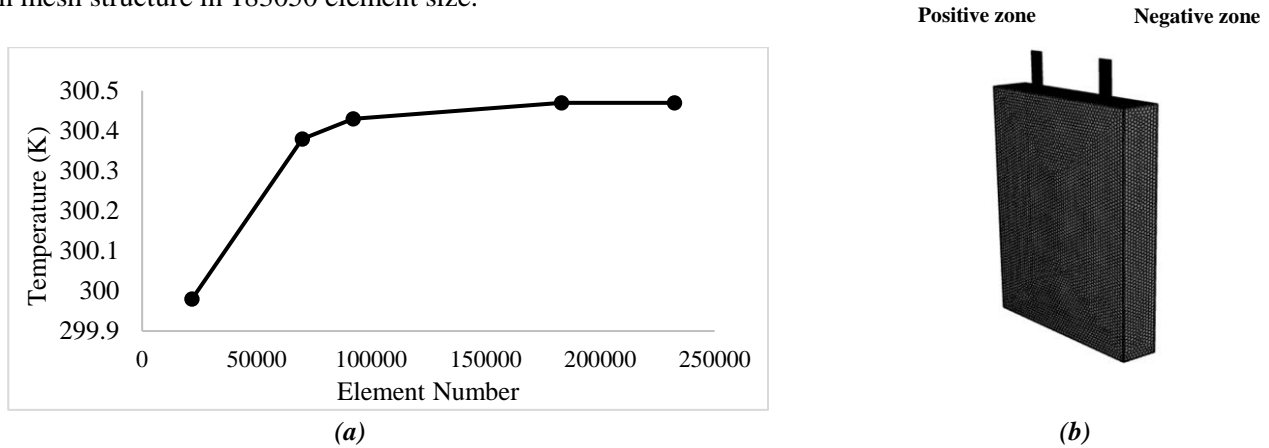


Fig 5. (a) Mesh independence for cell model; (b) Mesh structure in 183050 element size.

To verify the code, the average of measured temperature and voltage values during at 0.25C, 0.5C and 1C discharge rates was compared with the numerical model. Temperature and voltage results are shown in Fig. 6. and Fig. 7., respectively. According to increasing discharge C-rate, temperature values obtained from experimental data are 300.7K, 303.6K and 312.15K, and voltages are 2.77V, 2.76V, 2.75V. The temperature values obtained from numerical data are 300.44K, 304.84K, 313.39K, and voltages are 2.98V, 2.74V, 2.67V. The numerical model shows good agreement with experimental test data.

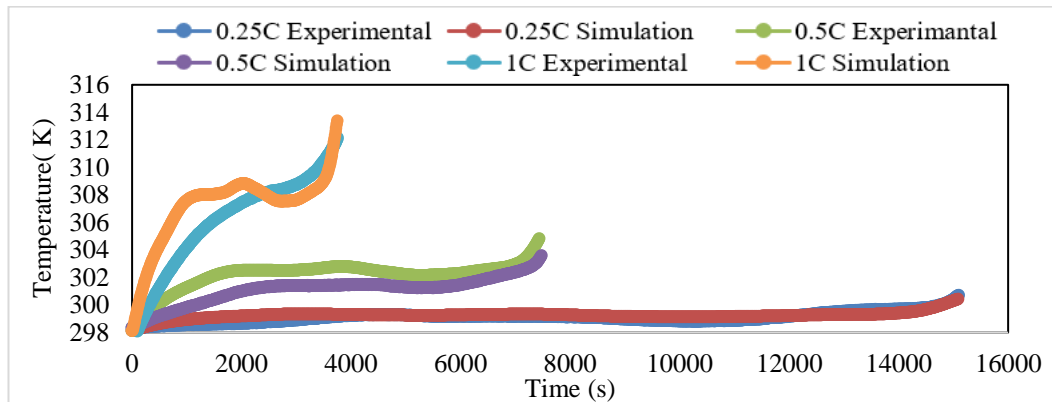


Fig 6. Average temperature profiles at 0.25C, 0.5C and 1C discharge rates.

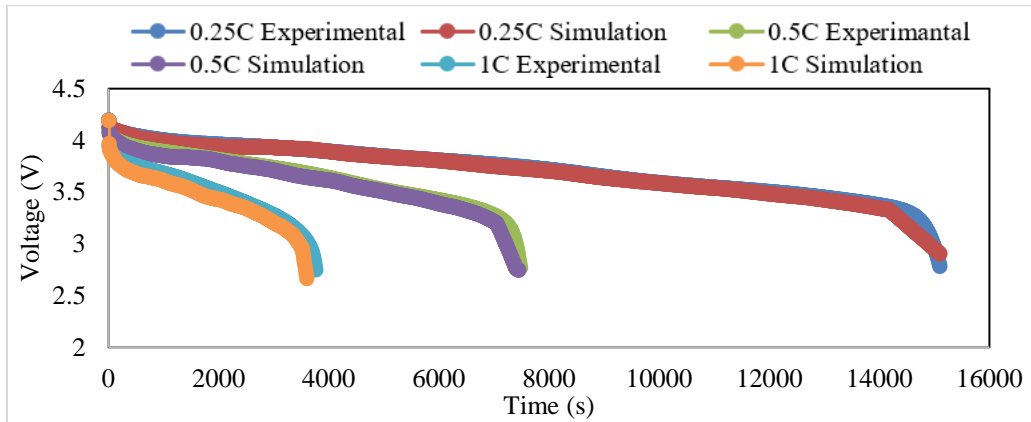
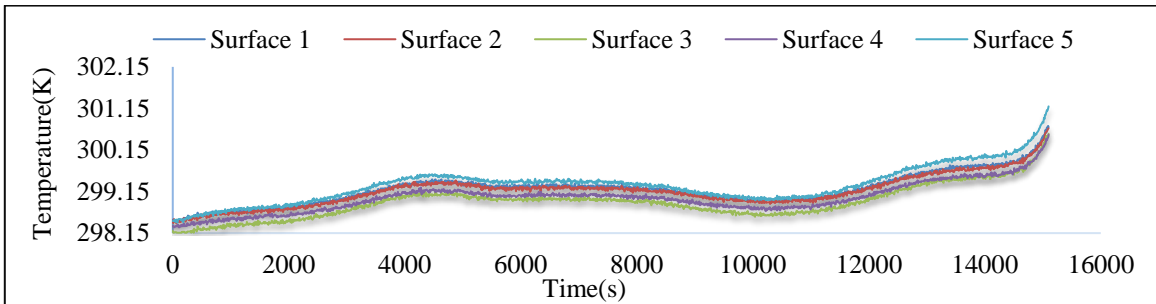


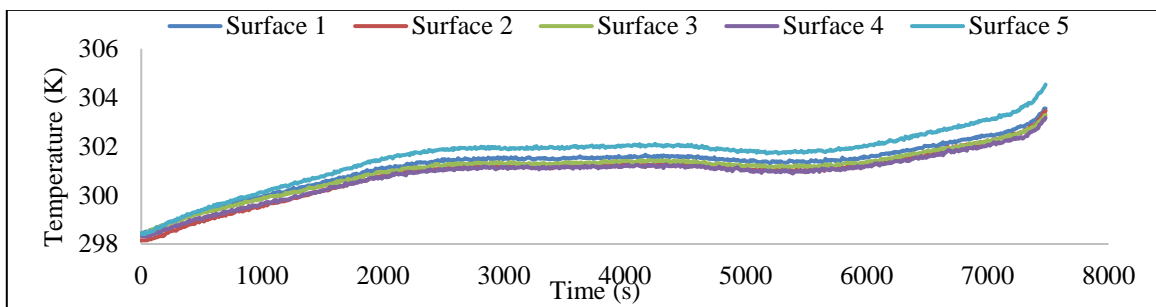
Fig 7. Voltage profiles at 0.25C, 0.5C and 1C discharge rates.

### 3. Result and Discussion

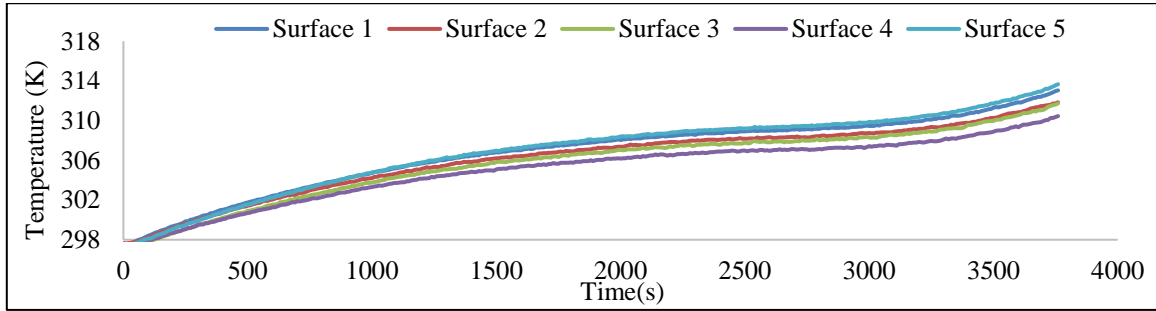
Fig. 8. shows temperature profiles measured on five different surfaces of the cell during discharge. The surface where the maximum temperature value is measured at all three different discharge rates is center of cell.



(a)



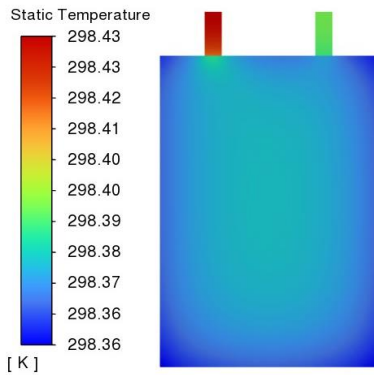
(b)



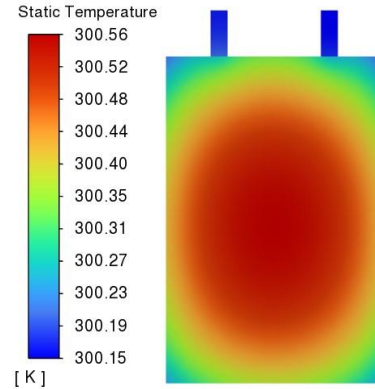
(c)

Fig 8. Surface temperature profiles at (a) 0.25C, (b) 0.5C and (c) 1C discharge rates.

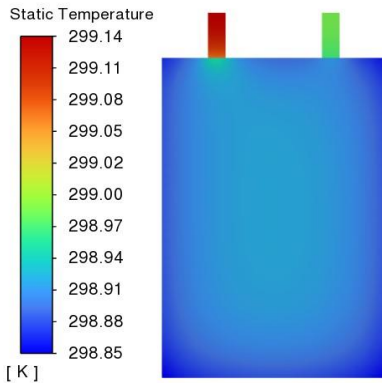
Fig. 9. shows the temperature profiles of cell during discharge. At the starting of the discharge, the hottest zone is represented by the cell external tabs, especially positive tab, in which the total current is conducted. This is explained by the ohmic heat generation which has a square dependency on the current applied. At higher C-rates, tabs are producing higher ohmic heat, hence they show higher temperature values in the applied discharge period. During discharge the hottest point of the battery passes from the external tabs to the battery center, which remains till the end of discharge. Also, it is observed that as the discharge rate increases, the temperature difference distribution across the cell surface increases.



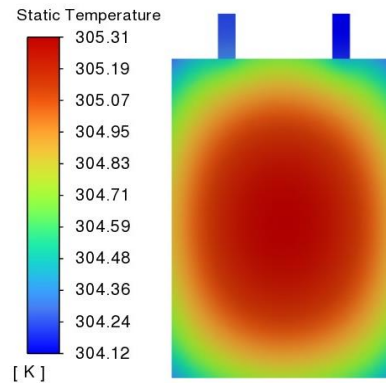
(a)



(d)



(b)



(e)

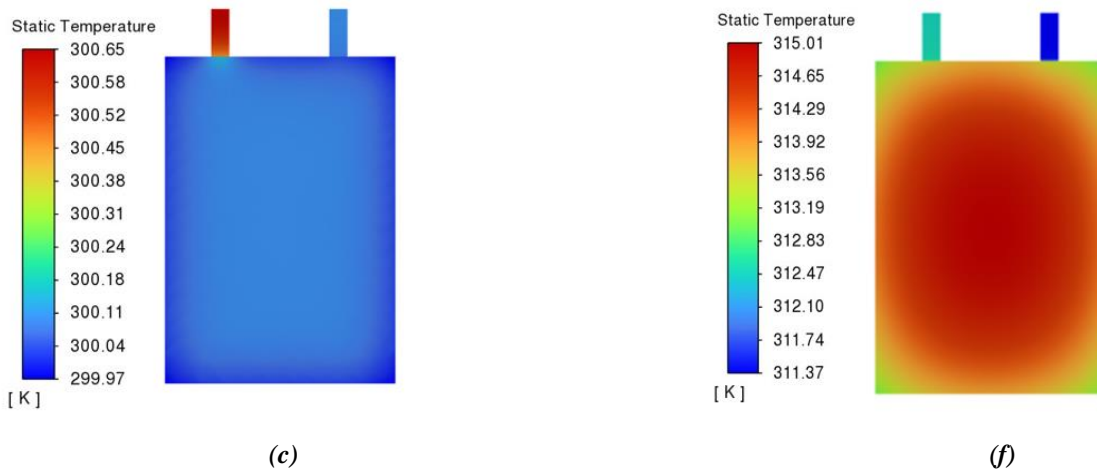


Fig 9. Temperature distribution of pouch cell (a) 0.25C discharge rate (at the end of  $t=180s$ ); (b) 0.5C discharge rate (at the end of  $t=180s$ ); (c) 1C discharge rate (at the end of  $t=180s$ ); (d) 0.25C discharge rate (at the end of discharge); (e) 0.5C discharge rate (at the end of discharge); (f) 1C discharge rate (at the end of discharge).

### 3. Conclusion

ECM-based three-dimensional thermal model was developed to analyse the thermal behaviour of a pouch-type NMC polymer Li-ion cell. Experimental and numerical tests performed in this study showed almost the same temperature and voltage profile throughout the cell's discharge at 0.25C, 0.5C and 1C. Numerical results suggest that maximum temperature obtained in external tabs at the beginning of the discharge, passes to the cell center throughout the discharge. The hot spot migration could be happening because of heat transfer convection at the cells tabs while the center is protected by the thin pouch cell cover.

In a conclusion because the coupling of a complex electro chemical-thermal model is computationally expensive, the ECM model can be effective in predicting the cell temperature profile for thermal management.

### References

- [1] V. Srinivasan, "Batteries for vehicular applications," American Institute of Physics, vol. 1044, pp. 283-296, 2008.
- [2] P. Sun, R. Bisschop, H. Niu, and X. Huang., "A Review of Battery Fires in Electric," Fire technology, pp. 1361-1410, 2020.
- [3] Q.L. Yue, C.X. He, M.C. Wu, T.S. Zhao, "Advances in thermal management systems for next-generation power batteries," International Journal of Heat and Mass Transfer, vol. 181, 2021.
- [4] E. Paccha-Herrera, W. R. Calderón-Muñoz, M. Orchard, F. Jaramillo, K. Medjaher, "Thermal Modeling Approaches for a LiCoO<sub>2</sub> Lithium-ion Battery—A Comparative Study with Experimental Validation," Batteries, p. 40, 2020.
- [5] J.H. Song, S.J. You, D.H. Jeon, "Numerical modeling and experimental validation of pouch-type," Journal of Applied Electrochemistry, vol. 44, pp. 1013-1023, 2014.
- [6] Q. Yang, J. Xu, B. Cao, X. Li, "A simplified fractional order impedance model and parameter identification method for lithium-ion batteries," PLoS One, 12(2), p. e0172424, 2017.
- [7] L. Sacchetti, "Electrochemical-thermal Analysis of High-Capacity Li-ion Pouch Cell for Automotive Applications," Department of Mechanical and Aerospace Engineering, Polytechnic University of Turin, Turin, Italy, 2020.